

SCP-Diff: Photo-Realistic Semantic Image Synthesis with Spatial-Categorical Joint Prior

Huan-ang Gao^{*1}, Mingju Gao^{*1}, Jiaju Li^{1,2}, Wenyi Li¹,
Rong Zhi³, Hao Tang⁴, and Hao Zhao^{†1}

¹ Institute for AI Industry Research (AIR), Tsinghua University

² University of Chinese Academy of Sciences

³ Mercedes-Benz Group China Ltd.

⁴ Carnegie Mellon University

gha20@mails.tsinghua.edu.cn, gaomingju19@mails.ucas.ac.cn

zhaohao@air.tsinghua.edu.cn

Project Page: <https://air-discover.github.io/SCP-Diff/>

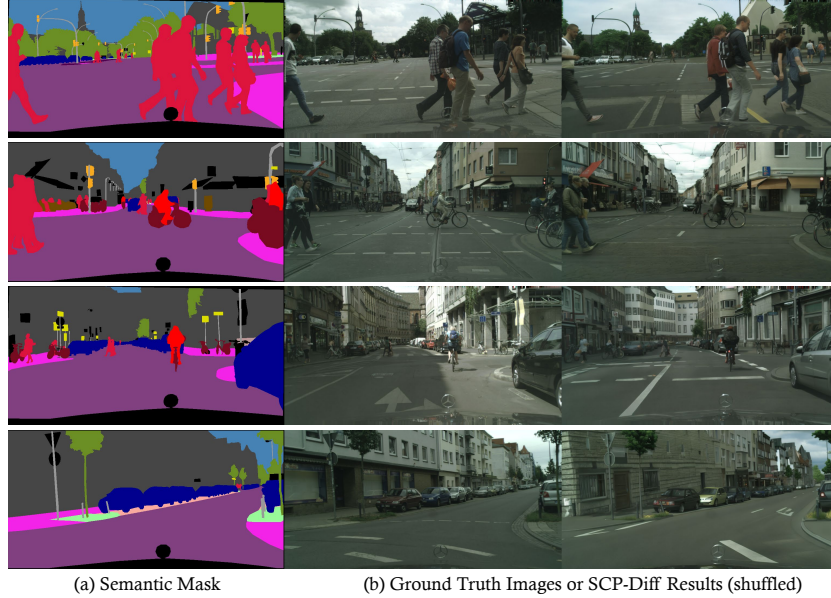


Fig. 1: For single-domain Cityscapes [8], our method can generate photo-realistic images from semantic masks (a). In (b), we shuffle ground truth real images and SCP-Diff results and the right answer is in the footnote of the conclusion. While the state-of-the-art method ECGAN [40] achieves 44.5 FID on Cityscapes, our method achieves 10.5 FID. The quality is credited to the strong spatial and categorical prior of Cityscapes.

Abstract. Semantic image synthesis (SIS) shows good promises for sensor simulation. However, current best practices in this field, based on GANs, have not yet reached the desired level of quality. As latent

¹ * Indicates Equal Contribution. [†] Indicates Corresponding Author.

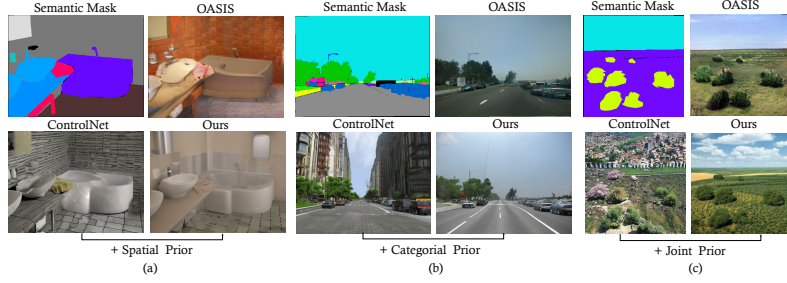


Fig. 2: We explain the underlying mechanisms of our proposed noise priors using ADE20K [59]. (a) Introducing the spatial prior aligns the image style with the dataset’s aesthetic while removing odd substructures in large semantic areas. (b) Incorporating the class prior can enhance alignment with the provided semantic masks. (c) By jointing spatial and class priors, their beneficial features are combined, allowing our joint prior (SCP-Diff) to achieve state-of-the-art results on ADE20K.

diffusion models make significant strides in image generation, we are prompted to evaluate ControlNet, a notable method for its dense control capabilities. Our investigation uncovered two primary issues with its results: the presence of weird sub-structures within large semantic areas and the misalignment of content with the semantic mask. Through empirical study, we pinpointed the cause of these problems as a mismatch between the noised training data distribution and the standard normal prior applied at the inference stage. To address this challenge, we developed specific noise priors for SIS, encompassing spatial, categorical, and an innovative spatial-categorical joint prior for inference. This approach, which we have named **SCP-Diff**, has yielded exceptional results, achieving an FID of 10.53 on Cityscapes and 12.66 on ADE20K. The code and models can be accessed via the project page.

Keywords: Semantic Image Synthesis · Diffusion Models · Noise Priors

1 Introduction

Semantic image synthesis is dedicated to generating high-quality images aligned with provided semantic maps, offering users the ability to accurately control the spatial layout of the generated images. The potential of this technology is particularly notable in fields like autonomous driving and robotics, because it enables the creation of highly realistic and diverse virtual environments with semantic layout control, reducing the dependency on extensive real-world data collection [20, 21, 25, 53, 58].

However, current leading techniques [33, 40] in this area, which rely on Generative Adversarial Networks (GANs), have not reached the anticipated quality levels necessary for the practical application of sensor simulation. As latent diffusion models achieve remarkable success in image creation, we are motivated to evaluate ControlNet [56], a method that enables dense control over Stable Diffusion [30]. We finetuned ControlNet with semantic label masks as conditions,

but identified two significant issues in the generated results: (i) the emergence of weird sub-structures in large semantic regions (see Fig. 2(a), the bathtub is divided into two parts) and (ii) the misalignment of content placement with the provided semantic masks (see Fig. 2(b), buildings appear in the sky region).

Why do large-scale pretrained latent diffusion models struggle to complete this semantic image synthesis task after finetuning? Our empirical analysis (see Fig. 3) reveals that the primary source of discrepancy in quality between the generated outcomes and the actual images is not from the score matching learning (*i.e.*, finetuning) process. Instead, it originates from a mismatch [17] between the distribution of noised data used during training and the standard normal distribution typically employed during the inference process.

Devise noise priors for inference. To address the mismatch in the distributions between training and inference, we implemented inference-time noise priors tailored for SIS, which can be seamlessly integrated into the finetuned ControlNet without further training. Initially, we introduced a spatial prior by estimating the distribution of real latents through a Gaussian model and averaging the outcomes across batches, similar to [11]. This approach notably improved the organization of scene layouts (for instance, the bathtub is now recognized as a single entity rather than fragmented parts in Fig. 2(a)) and enriched the diversity of colors observed in the images. This prior is closer to the training trajectory; however, discrepancies with the provided label masks remained evident (such as an unintended lamp appearing on the wall in Fig. 2(a)). We argue that this issue arises because the spatial noise prior unfits the control branch of ControlNet, where the former contains a mixture of modes (corresponding to different categories) during reduction, which may hinder the latter to generate meaningful residuals (added back to the SD branch) for *on-trajectory* denoising. To further refine our approach, we explored a categorical prior by aggregating real-image latents by class and started denoising from the aggregated statistics. This strategy helped reduce label alignment issues, though it resulted in the outputs reverting to a monotonous color scheme, as shown in Fig. 2(b).

To combine the best of both worlds, we introduced the Spatial-Categorical Joint Prior and coined this diffusion-based synthesis technique **SCP-Diff**. Our thorough experiments have confirmed the efficacy of SCP-Diff. Remarkably, despite its simplicity and the fact that it is training-free, SCP-Diff sets state-of-the-art on single-domain Cityscapes and multi-domain ADE20K simultaneously, synthesizes photo-realistic scenes that are difficult to distinguish from real ones (see Fig. 1, 2(c)). Aside from quality, we also quantitatively demonstrate that incorporating the prior does not negatively impact the diversity of diffusion-based generative modeling. User studies are also supportive for the quality and fidelity of the generated images to the provided label masks. The contributions of this work can be summarized as follows:

- We pinpoint the challenge posed by the discrepancy in inference distribution in finetuned ControlNets for Semantic Image Synthesis (SIS) and introduce a solution that utilizes inference noise priors to bridge this gap, notably without the need for retraining.

- We elucidate the design philosophy behind the creation of inference noise priors tailored for the SIS task, unpacking the mechanics of spatial and categorical priors within SIS, and finally integrate them into a joint one.
- Demonstrating superior capabilities, our integrated joint prior (SCP-Diff) achieves state-of-the-art performance on two well-established SIS benchmarks, Cityscapes and ADE20K, delivering high-quality outputs that are hard to distinguish from the real-world images.

2 Related Work

2.1 Semantic Image Synthesis

Semantic image synthesis (SIS) [19,23,26,42,43,46] aims to create photo-realistic images from semantic label maps. Previous works in this field are mostly based on Generative Adversarial Networks (GANs), which are trained using both adversarial loss [13] and reconstruction loss. A key advancement in network design was introduced with AdaIN [16], which aligns the mean and variance of content features with those of the style features. Building on this modulation concept, SPADE [26] proposes spatially adaptive normalization to better embed semantic layouts into the generator. CLADE [35] further optimized SPADE’s approach by introducing a more efficient normalization layer that adapts to different semantic classes. The state-of-the-art GAN-based approach, ECGAN [40], proposes to use the edge as an intermediate representation to help modulate the image generation process and employs contrastive learning to derive embeddings rich in semantic information.

The advent of conditional denoising diffusion probabilistic models [15,32] has spurred innovations in SIS. FreestyleNet [52] innovates within this space by adjusting the cross-attention maps, ensuring that each text token influences only the pixel regions delineated by the semantic mask. Following the modulation concept, SDM [47] designs a novel denoiser architecture with modulation layers. However, these methods directly operate in pixel space and, consequently, produce outcomes that are not as high-resolution as those generated by GAN-based techniques due to VRAM constraints.

2.2 Latent Diffusion-based Controllable Generation

Addressing the challenges of slow inference speeds and exceedingly high training expenses in pixel space, Stable Diffusion [30] introduced a two-stage image synthesis strategy. Initially, it employs VQGANs [10] to compress the image into a discretized latent code. Subsequently, it utilizes powerful diffusion-based generative modeling to process these latent representations, employing a UNet denoiser to exploit the inductive biases in images, which supports the text condition via cross attention. Building upon Stable Diffusion [30], numerous efforts aim to broaden control to additional modalities, such as incorporating CLIP features [29], or modifying specific regions through the inpainting formulation [1,9].

ControlNet [56] offers task-specific control by using a control branch to encode conditions. Within SIS, these conditions can be specified by color-coded semantic masks, and we report that such formulation can achieve state-of-the-art performance over previous SIS methods. Nevertheless, a more thorough examination uncovers issues such as the generation of unrealistic sub-structure and misalignment between the generated images and the corresponding semantic masks. This paper posits that the root cause of these issues lies in the initial noise setup and suggests the integration of the proposed pre-computed noise priors.

2.3 Playing Noise Tricks in Diffusion Models

Sampling Inversion. As DDIM sampling [32] operates deterministically, Null-text Inversion [24] learns to inverse this sampling process to extract noise from earlier timesteps, which is ideal for editing the signal image but not for generating new ones with label masks.

Signal Leakage in the Noised Latents. In video diffusion models, PYoCo [12] observed that the noise maps corresponding to frames from the same video tend to group together. FreeNoise [28] shows that rescheduling a sequence of noises enables long-range correlation modeling for longer video generation. These findings point to the assumption that common diffusion noise schedules inadequately corrupt signals in images, as discussed in [11]. To address this, FreeInit [50] refines the low-frequency components of the inference initial noise in an iterative manner in video diffusion models at the cost of inference time. [17] recommends retraining with a different noise schedule, which is computationally intensive. Note that none of these works specifically addresses SIS, where the key challenge is maintaining alignment with labels for controlled generation.

3 Preliminaries and Observations

3.1 Preliminaries

Given a semantic segmentation mask $M \in \mathbb{N}^{H \times W}$, where H and W represent height and width, and each element within M corresponds to a semantic label assigned to a specific pixel, the objective of semantic image synthesis (SIS) is to devise a function that transforms M into a photorealistic image $I \in \mathbb{R}^{H \times W \times 3}$.

The state-of-the-art method for SIS, ControlNet [56], is trained to reconstruct an initial image x_0 by removing noise from a distorted image x_t in a given timestep $t \in [0, T]$. At each timestep t , the denoising model ε_θ is presented with,

$$x_t = \sqrt{\alpha_t}x_0 + \sqrt{(1 - \alpha_t)}\varepsilon_t, \quad (1)$$

where x_0 is the image encoded by VQGAN [10] encoder, $\varepsilon_t \sim \mathcal{N}(0, I)$ and α_t is the cumulative product of scaling at each timestep t . Taking x_t as input, the denoising model predicts the added noise $\hat{\varepsilon}_t = \varepsilon_\theta(x_t, t, T, M)$, where T is the

encoding of the text condition and M is the label mask. Within the model, a non-trainable branch retains its configuration from the pretrained weights of Stable Diffusion [30] and is tasked with processing x_t, t , and T . Simultaneously, the model duplicates its encoder to a separate, trainable branch to process M , which is subsequently linked to the non-trainable one using layers of zero convolution. The loss function used to train the denoiser is defined as,

$$\mathcal{L} = \mathbb{E}_{x_0, t, T, M, \varepsilon_t} [\|\varepsilon_t - \hat{\varepsilon}_t\|^2]. \quad (2)$$

At inference time, we sample $x_T \sim \mathcal{N}_{\text{normal}}$, *i.e.*, $\mathcal{N}(0, I)$ and conduct the reverse denosing process iteratively from $t = T$ until $t = 1$,

$$x_{t-1} = \sqrt{\alpha_{t-1}} \left(\frac{x_t - \sqrt{1 - \alpha_t} \cdot \hat{\varepsilon}_t}{\sqrt{\alpha_t}} \right) + \sqrt{1 - \alpha_{t-1}} \cdot \hat{\varepsilon}_t. \quad (3)$$

After T iterations, we get x_0 and decode it to I using the VQGAN decoder [10].

3.2 Denoising from $\mathcal{N}_{\text{normal}}$? An Unreliable Inference Assumption

Simply applying ControlNet [56] finetuning to the Semantic Image Synthesis (SIS) task results in suboptimal outcomes, such as monotonous color schemes, weird substructures, or an inability to accurately follow semantic label masks, as illustrated in Figs. 2 and 7. To understand the underlying reasons for these issues, we perform an empirical analysis by finetuning on the ADE20K dataset. The results are reported in Fig. 3, where we try to analyze the errors associated with the generated results compared to the images from the ADE20K dataset.

We introduce $\mathcal{N}_{x_0, \mu T}$ as a means to investigate whether the score matching learning process, specifically the optimization of Eq. (2), incorporates any errors,

$$\mathcal{N}_{x_0, \mu T} := \mathcal{N}(\sqrt{\alpha_{\mu T}} x_0, (1 - \alpha_{\mu T}) I), \quad (4)$$

Intuitively, for each pair of (x_0, M) , we supply the denoising model with $x_{\mu T}$ (as defined in Eq. (1), $\mu \in [0, 1]$) and the condition branch with M , followed by assessing the resultant generation using the FID score. Although an increase in the FID score is expected with the progression of the denoising steps μT (Fig. 3(b)), a significant discrepancy (Fig. 3(a)) remains between the denoising from $\mathcal{N}_{x_0, T}$ ($\mu = 1$) and a standard denoising inference process, $\mathcal{N}_{\text{normal}}$.

The empirical study reveals that the common inference assumption that x_T should closely resemble $\mathcal{N}_{\text{normal}}$ is unreliable. This argument is also supported

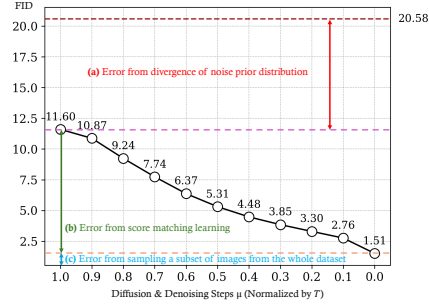


Fig. 3: An empirical study of denoising priors. Brown dotted line denotes the FID denoising from $\mathcal{N}_{\text{normal}}$, and the polyline illustrates the FID denoising from $\mathcal{N}_{x_0, \mu T}$ introduced in main text.

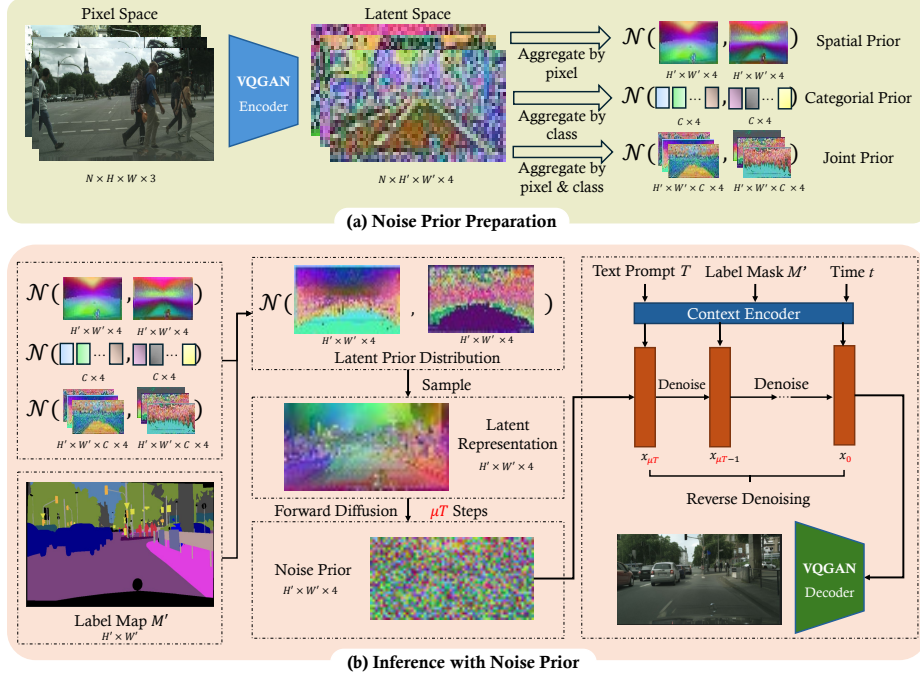


Fig. 4: Overview of our proposed framework. \mathcal{N} stands for Gaussian distribution.

by the mathematical analysis presented in [17, 55], arguing that current settings of α_t in practice can make the denoising model distinguish between initialization samples (namely x_T in our study) in training and testing cases. Nevertheless, their proposed solution, which involves retraining diffusion models, is costly and does not leverage important domain knowledge of semantic image synthesis, which demands (i) a comprehensive grasp of scene layouts from segmentation masks and (ii) adherence to pixel-wise dense semantic label maps at the same time.

4 Method

4.1 Overview

In Fig. 4, we provide an overview of our proposed framework, which is structured into two main stages: the preparation of latent priors and the application of these pre-computed latent priors during inference.

Noise Prior Preparation. With a set of N reference images, this phase involves reducing these images into latent priors, approximated by Gaussian distributions. Initially, the images are transformed into the latent space using a pretrained VQGAN [10] encoder, followed by computing the means and variances. Depending on the type of prior needed, we apply Eq. (5) for the spatial

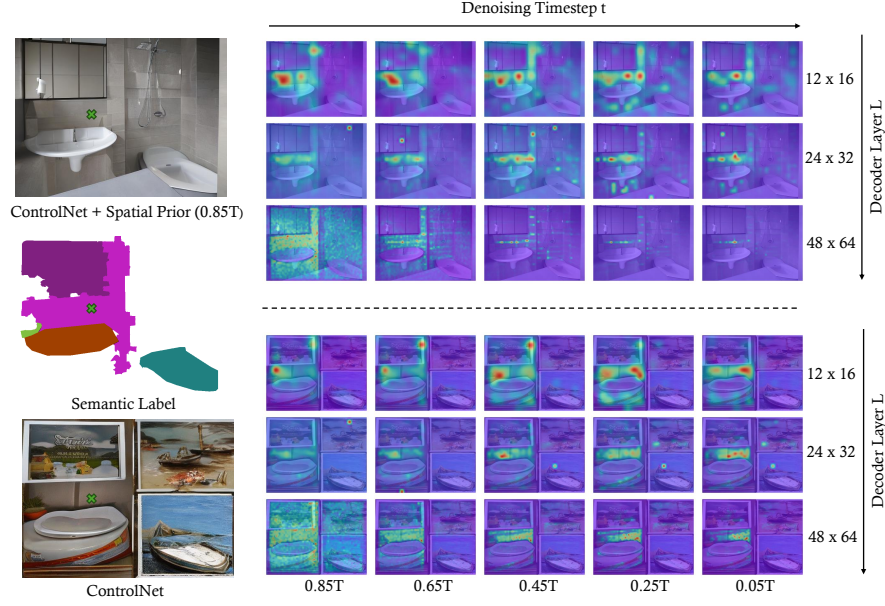


Fig. 5: Case study on spatial prior. We provided the finetuned ControlNet [56] with identical semantic label maps (middle on the left, where white pixels represent ‘unlabeled’), but introduced different priors, spatial prior (above) and normal prior (below). We visualize attention maps of decoder blocks where the query region is highlighted with a ‘X’. The images beneath the attention map masks represent the ultimate decoding outcomes and are included solely for visualization purposes.

prior, Eq. (7) for the categorical prior, and Eq. (8) for the joint version of the two.

Inference with Noise Prior. We first assemble the latent prior distribution map aligned with the provided downsampled label map M' . For the spatial prior, we directly replicate it. Otherwise, M' is used to index the specified prior on a token-by-token basis to construct a distribution map. From this distribution, we sample a latent representation and introduce noise for μT steps to create the noise prior. This noise prior is then processed through the fine-tuned ControlNet [56], which denoises the last μT steps. The final step involves utilizing the pretrained VQGAN [10] decoder to reconstruct the generated image.

4.2 Exploring Spatial Prior and Categorical Prior

With N reference latent images and their associated masks $\{(x_0^{(i)}, M^{(i)})\}_{i=1}^N$ from the dataset, our objective is to reduce them into noise priors $\mathcal{N}_{x_{\mu T}}$ which aligns with the training trajectory of noise distributions, facilitating low-error inference.

Spatial Prior. Given that the training process is focused on minimizing the score matching loss (Eq. (2)) for each instance of x_0 in expectation, with the theoretical premise that every x_0 has an equal impact on the ultimately learned

training noise distribution, our initial step is to diminish the reference latent images $\{x_0^{(i)}\}_{i=1}^N$ across the batch dimension.

More specifically, we define the spatial prior as,

$$\mathcal{N}_{\text{spatial}} := \mathcal{N} \left(\sum_{i=1}^N \frac{x_0^{(i)}}{N}, \left[\sum_{i=1}^N \frac{1}{N} \left[x_0^{(i)} - \mu(x_0^{(i)}) \right]^2 \right] \odot I_{H' \times W' \times 4} \right), \quad (5)$$

where \odot denotes the Hadamard product. For the sake of simplification in our reduction process, we choose not to model the correlations between spatial tokens collectively, treating each spatial location as an individual marginal distribution instead. For initializing noise values for the inference process started at μT , we sample from,

$$\mathcal{N}_{\text{spatial}, \mu T} := \mathcal{N} \left(\sqrt{\alpha_{\mu T}} \cdot x_{\text{spatial}}, (1 - \alpha_{\mu T}) I \right), \text{ where } x_{\text{spatial}} \sim \mathcal{N}_{\text{spatial}}. \quad (6)$$

So, what is encoded by the spatial prior? To answer this, we conducted a case study, illustrated in Fig. 5. From the analysis, we see that the group using spatial priors exhibits a broader receptive field in constructing scene layouts, in contrast to the group employing normal priors, which quickly focuses its attention narrowly on local fields. This distinction sheds light on why the spatial prior group can generate completed scenes with less weird sub-structures, while the normal prior group’s output resembles cropping and pasting objects following similar shape masks. Further insights from Fig. 7 demonstrate that the use of spatial priors facilitates the production of images that are consistent with the dataset style and enriched with a wider spectrum of colors and textures.

Categorical Prior. While spatial priors succeed in achieving global attention across the scene to construct scene layouts with fidelity, they fall short in incorporating class-specific information. This shortfall becomes apparent through hallucinatory artifacts, such as sketching buildings in the sky or drawing lamps on walls, as depicted in Fig. 2(a, b). We believe these hallucinations stem from the incompatibility between the spatial noise prior (which features a mix of class modes after reduction) and ControlNet’s control branch (which is only trained to denoise noised tokens of corresponding classes with the label mask). This mismatch confuses the control branch, leading to the generation of residuals (added back to the SD branch) that are less effective in denoising the current sample. Such errors accumulate along the denoising trajectory, potentially exacerbating the denoising process further away from the intended trajectory.

Therefore, we delve into the analysis of running statistics on a class-specific basis, calculating a categorical prior for each class. Initially, we downscale M to $M' \in \mathbb{N}^{H' \times W'}$ through nearest pixel selection, employing a scale factor of $\frac{H}{H'}$. Subsequently, for N reference images, we organize distinct sets N_c for each class c in the set of classes C , which comprise encoded tokens of dimension 1×4 . Following this, we compute the mean and standard deviation for each class to achieve a class-wise statistical reduction.

$$\mathcal{N}_{\text{categorical}, c} := \mathcal{N} \left(\text{Mean} [N_c], \text{Var} [N_c] \right). \quad (7)$$

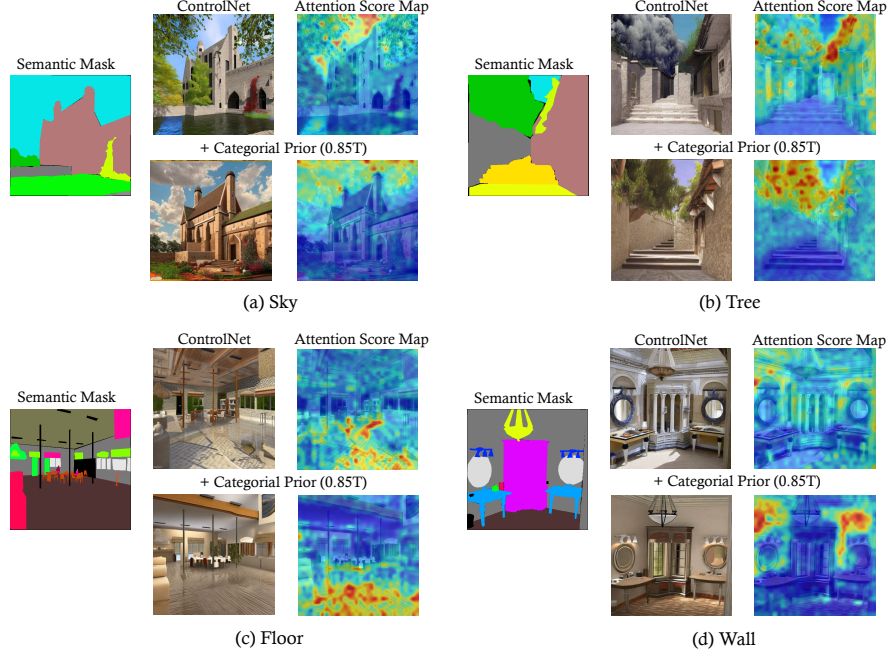


Fig. 6: Case study on categorical prior. We examine the intermediate features of encoder blocks from the middle of the denoising process where the object shapes begin to form [2, 4, 44]. The cross-attention score map is computed for these features against the language embeddings corresponding to various categories. It’s important to note that this extra categorical information from natural language is utilized solely for visualization and does *not* used in the actual denoising process. The denoiser exclusively identifies categories through the semantic mask and our categorical prior.

The definition of $\mathcal{N}_{\text{categorical},c,\mu T}$ is a replication of Eq. (6). To examine the knowledge encoded in the categorical prior, we also conduct a case study in Fig. 6. We find that the latent features denoised from the categorical prior achieve a multi-modal understanding of natural languages at the stage of object shaping. This can explain why our categorical prior can generate results that have better alignment with the given semantic mask. However, simply using the categorical prior makes the color scheme revert to a monotonous manner.

4.3 Joint Prior

In Sec. 4.2, we explore spatial prior, which aids in constructing scene layouts but falls short in generalizing to class-specific details, and class priors, which excel in generating localized objects of a certain class, yet lack comprehensive global attention. In this section, we introduce a combined prior that effectively merges these two aspects, which we dub as **joint prior**.

The calculation of the joint prior, $\mathcal{N}_{\text{joint}}$, can be formulated as follows. For N reference images, we use different sets $N_{x,y,c}$ to store encoded tokens with

dimensions 1×4 . Subsequently, the mean and variance are calculated for each tuple (x, y, c) , where $x \in [0, H'), y \in [0, W'), c \in C$,

$$\mathcal{N}_{\text{joint},x,y,c} := \mathcal{N}(\text{Mean}[N_{x,y,c}], \text{Var}[N_{x,y,c}]). \quad (8)$$

In instances where the sample size for a given tuple is excessively small, we revert to taking the statistics from class prior, assuming that such situations are rare and indicating a scenario where the local shape formation of an object should take precedence. The formulation of $\mathcal{N}_{\text{joint},x,y,c,\mu T}$ is also like Eq. (6). As evidenced by both quantitative (Tab. 1) and qualitative analyses (Fig. 7), the joint prior effectively incorporates the strengths of both spatial and categorical priors.

Discussion of Denoising steps μT . Ideally, the coefficient μ of the denoising timesteps needs to be carefully tuned. A smaller μ means injecting lower levels of noise into the calculated latent priors, thereby reducing the number of denoising steps required and accelerating the inference process. Nevertheless, within the framework of the joint prior, as we treat encoded tokens from varying spatial positions and categories as independent variables and overlook their correlations, a higher number of denoising steps μ becomes necessary. This requirement is due to the need for more self-attention to transition the marginal statistics towards joint modeling progressively. On a practical note, employing DDIM can expedite this search problem, significantly narrowing down the search space of μ -s to a stride of 0.05. We provide this study in Fig. 8.

5 Experiments

5.1 Setup

We evaluate our proposed noise priors on three challenging datasets: Cityscapes [8], ADE20K [59] and COCO-Stuff [3]. We use (i) the mean intersection-over-union (mIoU) and pixel accuracy (Acc) to evaluate the alignment with the provided label mask (following SPADE [26]), (ii) the Fréchet inception distance (FID) score [14] to access the quality of generated images, (iii) LPIPS [57] and MS-SSIM [49] to evaluate the diversity of generated images, and (iv) user study to see the aesthetic appeal of the outcomes.

We pre-compute the proposed priors on $N=10,000$ images. These latent priors are applied to ControlNet models [56] finetuned on three different datasets,

Table 1: Quantitative Comparison of Different Noise Priors.

Method	Cityscapes [8]			ADE20K [59]		
	mIoU \uparrow	Acc \uparrow	FID \downarrow	mIoU \uparrow	Acc \uparrow	FID \downarrow
Normal Prior	65.14 _(+0.00)	94.14 _(+0.00)	23.35 _(+0.00)	20.73 _(+0.00)	61.14 _(+0.00)	20.58 _(+0.00)
Spatial Prior	66.77 _(+1.63)	94.29 _(+0.15)	12.83 _(-10.52)	20.86 _(+0.13)	64.46 _(+3.32)	16.03 _(-4.55)
Categorical Prior	66.86 _(+1.72)	94.54 _(+0.40)	11.63 _(-11.72)	21.86 _(+1.13)	66.63 _(+5.49)	16.56 _(-4.02)
Joint Prior	67.92 _(+2.78)	94.65 _(+0.51)	10.53 _(-12.82)	25.61 _(+4.88)	71.79 _(+10.65)	12.66 _(-7.92)

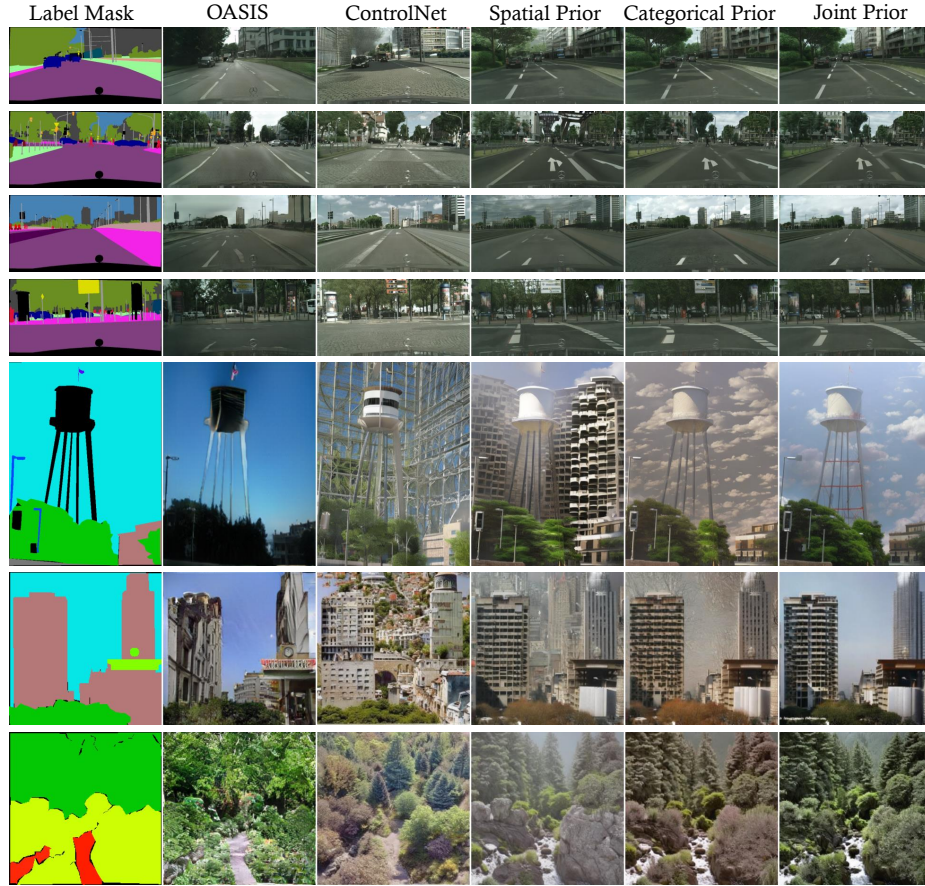


Fig. 7: Qualitative Comparison of Different Noise Priors. The resolutions for generated results on Cityscapes (top 4 rows) [8] and ADE20K (bottom 3 rows) [59] are 1024×512 and 512×512 , respectively. Please zoom in for a better view.

respectively. This finetuning process is conducted using a batch size of 16 on A100 80G GPUs, employing a learning rate of 10^{-5} across 100,000 steps. The decoder in the original Stable Diffusion [30] branch is also unlocked for tuning.

5.2 Main Results

Comparison of Noise Priors. In this section, we quantitatively and qualitatively compare different noise priors we proposed in this paper, including normal prior (which reduces to standard finetuned ControlNet [56] inference scheme), spatial prior, categorical prior and joint prior. The results are reported in Tab. 1 and Fig. 7.

Tab. 1 shows that the joint prior outperforms the standard inference prior of a normal distribution used by ControlNet [56] in terms of image quality (FID) and

consistency with the provided label masks (mIoU and Acc). For instance, on the Cityscapes dataset, our approach registers an improvement in mIoU of **+2.78** and a significant reduction in FID of **-12.82**. Examining the generated images more closely reveals that, while ControlNet (or the normal prior) tends to produce images with softer edges and fewer blur effects compared to OASIS, it struggles with scene layout organization and often fails to align correctly with the provided label masks, such as incorrectly placing buildings in the sky area. Conversely, our proposed joint prior addresses these issues, significantly enhancing photo-realism.

Comparison with State-of-the-Arts

Compared to state-of-the-art advancements in semantic image synthesis, our proposed joint prior (or SCP-Diff) maintains a competitive edge. As shown in Tab. 2, ControlNet [56] (or normal prior), by shifting the focus of generative modeling from pixel space to latent space, already significantly surpasses earlier methods, benefiting from the ability to synthesize high-resolution images. Our approach amplifies this advantage by addressing the issue of the inherent gap in the inference prior distribution of diffusion models, thus setting an astonishing low FID score for the Cityscapes [8] and ADE20K [59] datasets.

In the COCO-Stuff [3] dataset, our performance is on par with that of leading methods, despite achieving a significant improvement over ControlNet. This result can be attributed to the diverse spatial resolutions present within the COCO-Stuff dataset, requiring images to be resized into distorted shapes for processing by UNets, due to the requirement of denoising and diffusion processes for data of a uniform shape. Future research could explore solutions to this challenge.

By applying inference noise priors at μT where $\mu < 1$, we can optimize the traditionally time-consuming sampling method of latent diffusion models (which typically requires an amortized time of 2.34 seconds per image on A100 GPUs without any acceleration techniques) to a factor of μ . The selection of μ is ablated in the subsequent section.

Table 2: Comparison of Our Method with State-of-the-Art Approaches.

Method	FID		
	Cityscapes	ADE20K	COCO-Stuff
CRN [6]	104.7	73.3	70.4
SIMS [27]	49.7	-	-
Pix2pixHD [46]	95.0	81.8	111.5
GauGAN [26]	71.8	33.9	22.6
DPGAN [38]	53.0	31.7	-
DAGAN [36]	60.3	31.9	-
SelectionGAN [42]	65.2	33.1	-
SelectionGAN++ [41]	63.4	32.2	-
LGGAN [43]	57.7	31.6	-
LGGAN++ [39]	48.1	30.5	-
CC-FPSE [18]	54.3	31.7	19.2
INADE [34]	44.3	35.2	-
GroupDNet [60]	47.3	41.7	-
SC-GAN [48]	-	29.3	18.1
OASIS [33]	47.7	28.3	17.0
RESAIL [31]	45.5	30.2	18.3
SAFM [22]	49.5	32.8	24.6
ECGAN [37]	44.5	25.8	15.7
PITI [45]	-	27.9	16.1
FreestyleNet [52]	-	25.0	14.4
SDM [47]	42.1	27.5	15.9
ControlNet [56]	20.7	20.6	28.4
SCP-Diff (Joint prior)	10.5	13.0	17.6

Table 3: Diversity of Results.

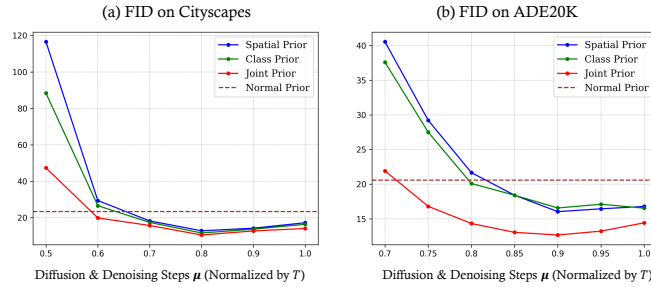
Method	ADE20K [59]	
	LPIPS \uparrow	MS-SSIM \downarrow
OASIS [33]	0.35	0.65
ControlNet [56]	0.59	0.17
SCP-Diff	<u>0.56</u>	<u>0.21</u>

Table 4: Results of User Study.

Method	Result Quality \uparrow	Condition Fidelity \uparrow
OASIS [33]	1.45 ± 0.48	1.65 ± 0.59
ControlNet [56]	1.93 ± 0.46	1.80 ± 0.52
SCP-Diff	2.62 ± 0.36	2.55 ± 0.43

5.3 Study on Denoising Steps μT

As discussed in Sec. 4.3, we conducted an experiment to see the effect of μT over the quality of the generated results. From Fig. 8, we can see that the optimal choice of μ for quality lies in $[0.8, 0.9]$ for both datasets. The trend patterns observed in both curves are similar, indicating a level of robustness when applying noise priors.

Fig. 8: Study on the Effects of Denoising Steps μT .

5.4 Study on Diversity of Generated Results

Following OASIS [33], we assess the diversity of the generated images by analyzing the variation within a set of images created from the same label map, referred to as a batch, using MS-SSIM and LPIPS. We produce 20 images per label map, calculate the mean pairwise scores across these images, and then average these scores over the label maps. Intuitively, the larger differences among images within the same batch indicate a higher diversity in the generated outcomes. From the results in Tab. 3, we see that our joint prior registers a marginally reduced diversity score compared to ControlNet [56]. This outcome is anticipated, considering that introducing priors to the inference process inherently balances diversity against improved quality.

5.5 User Study

Following ControlNet [56], we conduct a user study and invite participants to rank 500 groups of images generated by three methods (see Tab. 4) individually

in terms of “the quality of displayed images” and “the fidelity to the given label mask”. We employ the Average Human Ranking (AHR) as a metric for user preference, where participants rank each result on a scale from 1 to 3, with 3 being the best. According to the average rankings shown in Tab. 4, users significantly favor the outcomes produced by our method over those generated by ControlNet [56].

6 Conclusion

In this paper, we have addressed the challenge of the inference distribution discrepancy in finetuned ControlNets for Semantic Image Synthesis (SIS) by introducing inference noise priors that effectively bridge this gap, eliminating the need for retraining. We devised inference noise priors tailored for SIS and delved into the design philosophy and mechanics behind them, exploring both spatial and categorical priors before successfully integrating them into a comprehensive joint prior. Our SCP-Diff showcases outstanding performance, setting new benchmarks in SIS on two prominent datasets, Cityscapes and ADE20K. We hope our insights and high-quality generated images will inspire future works in the research community.²³

References

1. Avrahami, O., Lischinski, D., Fried, O.: Blended diffusion for text-driven editing of natural images. In: Proceedings of the IEEE/CVF Conference on Computer Vision and Pattern Recognition. pp. 18208–18218 (2022) 4
2. Balaji, Y., Nah, S., Huang, X., Vahdat, A., Song, J., Kreis, K., Aittala, M., Aila, T., Laine, S., Catanzaro, B., et al.: ediffi: Text-to-image diffusion models with an ensemble of expert denoisers. arXiv preprint arXiv:2211.01324 (2022) 10
3. Caesar, H., Uijlings, J., Ferrari, V.: Coco-stuff: Thing and stuff classes in context. In: Proceedings of the IEEE conference on computer vision and pattern recognition. pp. 1209–1218 (2018) 11, 13, 19
4. Cao, M., Wang, X., Qi, Z., Shan, Y., Qie, X., Zheng, Y.: Masactrl: Tuning-free mutual self-attention control for consistent image synthesis and editing. arXiv preprint arXiv:2304.08465 (2023) 10
5. Chen, L.C., Papandreou, G., Kokkinos, I., Murphy, K., Yuille, A.L.: Semantic image segmentation with deep convolutional nets and fully connected crfs. arXiv preprint arXiv:1412.7062 (2014) 19
6. Chen, Q., Koltun, V.: Photographic image synthesis with cascaded refinement networks. In: Proceedings of the IEEE international conference on computer vision. pp. 1511–1520 (2017) 13
7. Chong, M.J., Forsyth, D.: Effectively unbiased fid and inception score and where to find them. arXiv preprint arXiv:1911.07023 (2019) 19

² The real images in Fig. 1 are all in the left.

³ This research is supported by Tsinghua University – Mercedes Benz Institute for Sustainable Mobility.

8. Cordts, M., Omran, M., Ramos, S., Rehfeld, T., Enzweiler, M., Benenson, R., Franke, U., Roth, S., Schiele, B.: The cityscapes dataset for semantic urban scene understanding. In: Proceedings of the IEEE conference on computer vision and pattern recognition. pp. 3213–3223 (2016) [1](#), [11](#), [12](#), [13](#), [19](#)
9. Couairon, G., Verbeek, J., Schwenk, H., Cord, M.: Diffedit: Diffusion-based semantic image editing with mask guidance. arXiv preprint arXiv:2210.11427 (2022) [4](#)
10. Esser, P., Rombach, R., Ommer, B.: Taming transformers for high-resolution image synthesis. In: Proceedings of the IEEE/CVF conference on computer vision and pattern recognition. pp. 12873–12883 (2021) [4](#), [5](#), [6](#), [7](#), [8](#)
11. Everaert, M.N., Fitsios, A., Bocchio, M., Arpa, S., Süssstrunk, S., Achanta, R.: Exploiting the signal-leak bias in diffusion models. In: Proceedings of the IEEE/CVF Winter Conference on Applications of Computer Vision. pp. 4025–4034 (2024) [3](#), [5](#)
12. Ge, S., Nah, S., Liu, G., Poon, T., Tao, A., Catanzaro, B., Jacobs, D., Huang, J.B., Liu, M.Y., Balaji, Y.: Preserve your own correlation: A noise prior for video diffusion models. In: Proceedings of the IEEE/CVF International Conference on Computer Vision. pp. 22930–22941 (2023) [5](#)
13. Goodfellow, I., Pouget-Abadie, J., Mirza, M., Xu, B., Warde-Farley, D., Ozair, S., Courville, A., Bengio, Y.: Generative adversarial networks. Communications of the ACM **63**(11), 139–144 (2020) [4](#)
14. Heusel, M., Ramsauer, H., Unterthiner, T., Nessler, B., Hochreiter, S.: Gans trained by a two time-scale update rule converge to a local nash equilibrium. Advances in neural information processing systems **30** (2017) [11](#)
15. Ho, J., Jain, A., Abbeel, P.: Denoising diffusion probabilistic models. Advances in neural information processing systems **33**, 6840–6851 (2020) [4](#)
16. Huang, X., Belongie, S.: Arbitrary style transfer in real-time with adaptive instance normalization. In: Proceedings of the IEEE international conference on computer vision. pp. 1501–1510 (2017) [4](#)
17. Lin, S., Liu, B., Li, J., Yang, X.: Common diffusion noise schedules and sample steps are flawed. In: Proceedings of the IEEE/CVF Winter Conference on Applications of Computer Vision. pp. 5404–5411 (2024) [3](#), [5](#), [7](#)
18. Liu, X., Yin, G., Shao, J., Wang, X., et al.: Learning to predict layout-to-image conditional convolutions for semantic image synthesis. Advances in Neural Information Processing Systems **32** (2019) [13](#)
19. Lu, M., Zhao, H., Yao, A., Chen, Y., Xu, F., Zhang, L.: A closed-form solution to universal style transfer. In: Proceedings of the IEEE/CVF International Conference on Computer Vision. pp. 5952–5961 (2019) [4](#)
20. Luo, W., Yang, S., Wang, H., Long, B., Zhang, W.: Context-consistent semantic image editing with style-preserved modulation. In: European Conference on Computer Vision. pp. 561–578. Springer (2022) [2](#)
21. Luo, W., Yang, S., Zhang, X., Zhang, W.: Siedob: Semantic image editing by disentangling object and background. In: Proceedings of the IEEE/CVF Conference on Computer Vision and Pattern Recognition. pp. 1868–1878 (2023) [2](#)
22. Lv, Z., Li, X., Niu, Z., Cao, B., Zuo, W.: Semantic-shape adaptive feature modulation for semantic image synthesis. In: Proceedings of the IEEE/CVF Conference on Computer Vision and Pattern Recognition. pp. 11214–11223 (2022) [13](#)
23. Lv, Z., Wei, Y., Zuo, W., Wong, K.Y.K.: Place: Adaptive layout-semantic fusion for semantic image synthesis (2024) [4](#)

24. Mokady, R., Hertz, A., Aberman, K., Pritch, Y., Cohen-Or, D.: Null-text inversion for editing real images using guided diffusion models. In: Proceedings of the IEEE/CVF Conference on Computer Vision and Pattern Recognition. pp. 6038–6047 (2023) [5](#)
25. Ntavelis, E., Romero, A., Kastanis, I., Van Gool, L., Timofte, R.: Sesame: Semantic editing of scenes by adding, manipulating or erasing objects. In: Computer Vision–ECCV 2020: 16th European Conference, Glasgow, UK, August 23–28, 2020, Proceedings, Part XXII 16. pp. 394–411. Springer (2020) [2](#)
26. Park, T., Liu, M.Y., Wang, T.C., Zhu, J.Y.: Semantic image synthesis with spatially-adaptive normalization. In: Proceedings of the IEEE/CVF conference on computer vision and pattern recognition. pp. 2337–2346 (2019) [4](#), [11](#), [13](#)
27. Qi, X., Chen, Q., Jia, J., Koltun, V.: Semi-parametric image synthesis. In: Proceedings of the IEEE Conference on Computer Vision and Pattern Recognition. pp. 8808–8816 (2018) [13](#)
28. Qiu, H., Xia, M., Zhang, Y., He, Y., Wang, X., Shan, Y., Liu, Z.: Freenoise: Tuning-free longer video diffusion via noise rescheduling. arXiv preprint arXiv:2310.15169 (2023) [5](#)
29. Ramesh, A., Dhariwal, P., Nichol, A., Chu, C., Chen, M.: Hierarchical text-conditional image generation with clip latents. arXiv preprint arXiv:2204.06125 1(2), 3 (2022) [4](#)
30. Rombach, R., Blattmann, A., Lorenz, D., Esser, P., Ommer, B.: High-resolution image synthesis with latent diffusion models. In: Proceedings of the IEEE/CVF conference on computer vision and pattern recognition. pp. 10684–10695 (2022) [2](#), [4](#), [6](#), [12](#)
31. Shi, Y., Liu, X., Wei, Y., Wu, Z., Zuo, W.: Retrieval-based spatially adaptive normalization for semantic image synthesis. In: Proceedings of the IEEE/CVF Conference on Computer Vision and Pattern Recognition. pp. 11224–11233 (2022) [13](#)
32. Song, J., Meng, C., Ermon, S.: Denoising diffusion implicit models. arXiv preprint arXiv:2010.02502 (2020) [4](#), [5](#)
33. Sushko, V., Schönfeld, E., Zhang, D., Gall, J., Schiele, B., Khoreva, A.: Oasis: only adversarial supervision for semantic image synthesis. International Journal of Computer Vision **130**(12), 2903–2923 (2022) [2](#), [13](#), [14](#), [19](#)
34. Tan, Z., Chai, M., Chen, D., Liao, J., Chu, Q., Liu, B., Hua, G., Yu, N.: Diverse semantic image synthesis via probability distribution modeling. In: Proceedings of the IEEE/CVF Conference on Computer Vision and Pattern Recognition. pp. 7962–7971 (2021) [13](#)
35. Tan, Z., Chen, D., Chu, Q., Chai, M., Liao, J., He, M., Yuan, L., Hua, G., Yu, N.: Efficient semantic image synthesis via class-adaptive normalization. IEEE Transactions on Pattern Analysis and Machine Intelligence **44**(9), 4852–4866 (2021) [4](#)
36. Tang, H., Bai, S., Sebe, N.: Dual attention gans for semantic image synthesis. In: Proceedings of the 28th ACM International Conference on Multimedia. pp. 1994–2002 (2020) [13](#)
37. Tang, H., Qi, X., Sun, G., Xu, D., Sebe, N., Timofte, R., Van Gool, L.: Edge guided gans with contrastive learning for semantic image synthesis. arXiv preprint arXiv:2003.13898 (2020) [13](#)
38. Tang, H., Sebe, N.: Layout-to-image translation with double pooling generative adversarial networks. IEEE Transactions on Image Processing **30**, 7903–7913 (2021) [13](#)

39. Tang, H., Shao, L., Torr, P.H., Sebe, N.: Local and global gans with semantic-aware upsampling for image generation. *IEEE Transactions on Pattern Analysis and Machine Intelligence* **45**(1), 768–784 (2022) [13](#)
40. Tang, H., Sun, G., Sebe, N., Van Gool, L.: Edge guided gans with multi-scale contrastive learning for semantic image synthesis. *IEEE Transactions on Pattern Analysis and Machine Intelligence* (2023) [1](#), [2](#), [4](#)
41. Tang, H., Torr, P.H., Sebe, N.: Multi-channel attention selection gans for guided image-to-image translation. *IEEE Transactions on Pattern Analysis and Machine Intelligence* **45**(5), 6055–6071 (2022) [13](#)
42. Tang, H., Xu, D., Sebe, N., Wang, Y., Corso, J.J., Yan, Y.: Multi-channel attention selection gan with cascaded semantic guidance for cross-view image translation. In: *Proceedings of the IEEE/CVF conference on computer vision and pattern recognition*. pp. 2417–2426 (2019) [4](#), [13](#)
43. Tang, H., Xu, D., Yan, Y., Torr, P.H., Sebe, N.: Local class-specific and global image-level generative adversarial networks for semantic-guided scene generation. In: *Proceedings of the IEEE/CVF conference on computer vision and pattern recognition*. pp. 7870–7879 (2020) [4](#), [13](#)
44. Voynov, A., Chu, Q., Cohen-Or, D., Aberman, K.: $p+$: Extended textual conditioning in text-to-image generation. *arXiv preprint arXiv:2303.09522* (2023) [10](#)
45. Wang, T., Zhang, T., Zhang, B., Ouyang, H., Chen, D., Chen, Q., Wen, F.: Pretraining is all you need for image-to-image translation. *arXiv preprint arXiv:2205.12952* (2022) [13](#)
46. Wang, T.C., Liu, M.Y., Zhu, J.Y., Tao, A., Kautz, J., Catanzaro, B.: High-resolution image synthesis and semantic manipulation with conditional gans. In: *Proceedings of the IEEE conference on computer vision and pattern recognition*. pp. 8798–8807 (2018) [4](#), [13](#)
47. Wang, W., Bao, J., Zhou, W., Chen, D., Chen, D., Yuan, L., Li, H.: Semantic image synthesis via diffusion models. *arXiv preprint arXiv:2207.00050* (2022) [4](#), [13](#)
48. Wang, Y., Qi, L., Chen, Y.C., Zhang, X., Jia, J.: Image synthesis via semantic composition. In: *Proceedings of the IEEE/CVF International Conference on Computer Vision*. pp. 13749–13758 (2021) [13](#)
49. Wang, Z., Simoncelli, E.P., Bovik, A.C.: Multiscale structural similarity for image quality assessment. In: *The Thirty-Seventh Asilomar Conference on Signals, Systems & Computers, 2003*. vol. 2, pp. 1398–1402. Ieee (2003) [11](#)
50. Wu, T., Si, C., Jiang, Y., Huang, Z., Liu, Z.: Freeinit: Bridging initialization gap in video diffusion models. *arXiv preprint arXiv:2312.07537* (2023) [5](#)
51. Xiao, T., Liu, Y., Zhou, B., Jiang, Y., Sun, J.: Unified perceptual parsing for scene understanding. In: *Proceedings of the European conference on computer vision (ECCV)*. pp. 418–434 (2018) [19](#)
52. Xue, H., Huang, Z., Sun, Q., Song, L., Zhang, W.: Freestyle layout-to-image synthesis. In: *Proceedings of the IEEE/CVF Conference on Computer Vision and Pattern Recognition*. pp. 14256–14266 (2023) [4](#), [13](#)
53. Yang, L., Xu, X., Kang, B., Shi, Y., Zhao, H.: Freemask: Synthetic images with dense annotations make stronger segmentation models. *Advances in Neural Information Processing Systems* **36** (2024) [2](#)
54. Yu, F., Koltun, V., Funkhouser, T.: Dilated residual networks. In: *Proceedings of the IEEE conference on computer vision and pattern recognition*. pp. 472–480 (2017) [19](#)
55. Zhang, J., Chang, S.Y., Li, K., Forsyth, D.: Preserving image properties through initializations in diffusion models. In: *Proceedings of the IEEE/CVF Winter Conference on Applications of Computer Vision*. pp. 5242–5250 (2024) [7](#)

56. Zhang, L., Rao, A., Agrawala, M.: Adding conditional control to text-to-image diffusion models. In: Proceedings of the IEEE/CVF International Conference on Computer Vision. pp. 3836–3847 (2023) 2, 5, 6, 8, 11, 12, 13, 14, 15, 19
57. Zhang, R., Isola, P., Efros, A.A., Shechtman, E., Wang, O.: The unreasonable effectiveness of deep features as a perceptual metric. In: CVPR (2018) 11
58. Zheng, Y., Zhong, C., Li, P., Gao, H.a., Zheng, Y., Jin, B., Wang, L., Zhao, H., Zhou, G., Zhang, Q., et al.: Steps: Joint self-supervised nighttime image enhancement and depth estimation. arXiv preprint arXiv:2302.01334 (2023) 2
59. Zhou, B., Zhao, H., Puig, X., Fidler, S., Barriuso, A., Torralba, A.: Scene parsing through ade20k dataset. In: Proceedings of the IEEE conference on computer vision and pattern recognition. pp. 633–641 (2017) 2, 11, 12, 13, 14, 19
60. Zhu, Z., Xu, Z., You, A., Bai, X.: Semantically multi-modal image synthesis. In: Proceedings of the IEEE/CVF conference on computer vision and pattern recognition. pp. 5467–5476 (2020) 13

A Implementation Details

Finetuning ControlNet. We initialize the Stable Diffusion branch of ControlNet [56] with SD 2.1 weights. During training, we set the text prompt to fixed strings, and those are: *City road scenes* for Cityscapes [8], *Photorealistic and diverse images depicting various scenes* for ADE20K [59], and *high quality, detailed* for COCO-Stuff [3]. This aims to ensure that the text prompt remains devoid of any semantic cues, with the sole source of semantics derived from the semantic label processed by the control branch and the noise priors.

Evaluation. During inference of the generated results from different datasets, the text prompt was kept the same as the training procedure. For evaluation of FID, we sampled 50,000 images for each group of experimental setting, noting that FID score is biased and the bias is depending on the number of images we use for calculation [7]. For evaluation of mIoU, we follow OASIS [33], using UperNet101 [51] for ADE20K, multi-scale DRN-D-105 [54] for Cityscapes, and DeepLabV2 [5] for COCO-Stuff.

B Results

We provide more qualitative results, with Fig. 9 and Fig. 10 for Cityscapes, Fig. 11 and Fig. 12 for ADE20K, Fig. 13 and Fig. 14 for COCO-Stuff.



Fig. 9: Qualitative Results on Cityscapes dataset. (cont.)



Fig. 10: Qualitative Results on Cityscapes dataset. (cont.)



Fig. 11: Qualitative Results on ADE20K dataset. (cont.)

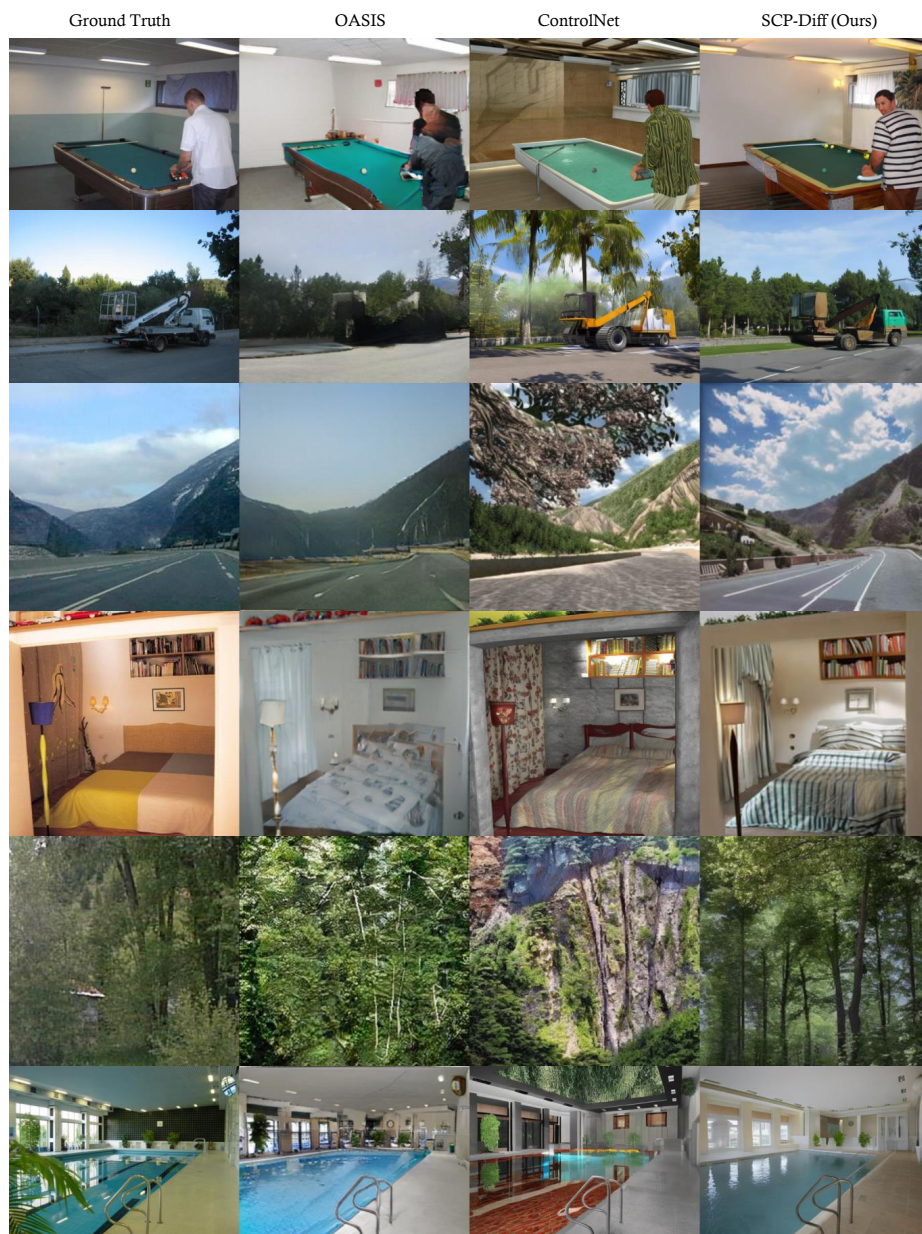


Fig. 12: Qualitative Results on ADE20K dataset. (cont.)

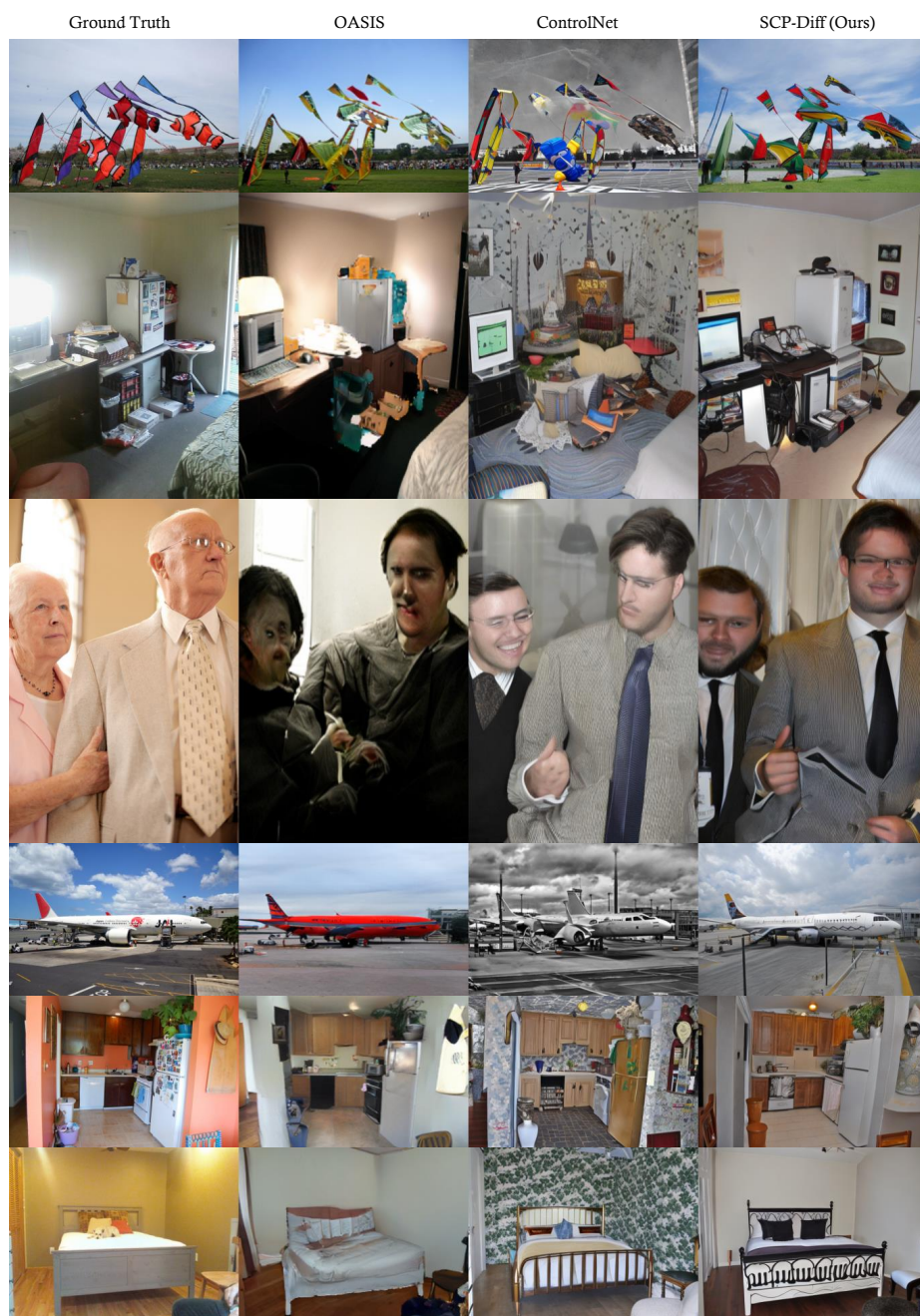


Fig. 13: Qualitative Results on COCO-Stuff dataset. (cont.)



Fig. 14: Qualitative Results on COCO-Stuff dataset.